A Comparison of Rotordynamic-Coefficient Predictions for Annular Honeycomb Gas Seals Using Three Different Friction-Factor Models

Rohan J. D'Souza
Graduate Research Assistant

Dara W. Childs
Leland T. Jordan Professor
of Mechanical Engineering

Turbomachinery Laboratory,
Texas A&M University,
College Station, TX 77843

A two-control-volume bulk-flow model is used to predict rotordynamic coefficients for an annular, honeycomb-stator/smooth-rotor gas seal. The bulk-flow model uses Hirs' turbulent-lubrication model, which requires a friction factor model to define the shear stresses at the rotor and stator wall. Rotordynamic coefficients predictions are compared for the following three variations of the Blasius pipe-friction model: (i) a basic model where the Reynolds number is a linear function of the local clearance, $f_s = n_s Re^{m_s}$ (ii) a model where the coefficient is a function of the local clearance, and (iii) a model where both the coefficient and exponent are functions of the local clearance. The latter models are based on data that shows the friction factor increasing with increasing clearances. Rotordynamic-coefficient predictions shows that the friction-factor-model choice is important in predicting the effective-damping coefficients at a lower frequency range (60~70 Hz) where industrial centrifugal compressors and steam turbines tend to become unstable. At a higher frequency range, irrespective of the friction-factor model, the rotordynamic-coefficient predictions tend to coincide. Blasius-based Models which directly account for the observed increase in stator friction factors with increasing clearance predict significantly lower values for the destabilizing cross-coupled stiffness coefficients.
[DOI: 10.1115/1.1456086]

Introduction

Turbomachinery annular seals are provided to limit leakage between regions at different pressures. Seals increase the efficiency of turbomachines; however, they can also significantly influence the rotordynamics of high performance turbomachinery. Centrifugal injection compressors use honeycomb stators with smooth rotors, Fig. 1. This configuration provides good leakage control as well as improved stability by increasing the seal's effective damping and is the subject of this paper. Aircraft gas turbines regularly use honeycomb stators as an abradable element with a tooth-on-rotor labyrinth seal. As speed increases, the labyrinth teeth diameters grow, and the teeth tips cut into the honeycomb stator. This configuration reduces leakage but does not improve rotordynamic stability.

Childs and Moyer [2] cited the elimination of an instability for the High Pressure Oxygen Turbopump of the Space Shuttle Main Engine by changing the turbine interstage seal from a stepped-labyrinth, tooth-on-rotor configuration to a smooth-rotor, honeycomb-stator configuration. Zeidan et al. [3] and Armstrong and Perricone [4] presented case studies where rotordynamic instabilities were eliminated in centrifugal compressors and a steam turbine by replacing tooth-on-stator labyrinth seals with smooth-rotor/honeycomb stator seals. Numerous subsequent papers have documented the successful elimination of rotordynamic instabilities via this type of seal replacement.

In relation to dynamics of rotating machinery, annular gas seals have been modeled traditionally by stiffness and damping coefficients, expressed as

$$-\begin{Bmatrix} F_x \\ F_y \end{Bmatrix} = \begin{bmatrix} K & k \\ -k & K \end{bmatrix} \begin{Bmatrix} x \\ y \end{Bmatrix} + \begin{bmatrix} C & c \\ -c & C \end{bmatrix} \begin{Bmatrix} \dot{x} \\ \dot{y} \end{Bmatrix}. \quad (1)$$

The direct stiffness K and direct damping C terms account for a reaction force in the direction of motion. The cross-coupled stiffness k and cross-coupled damping c terms develop reaction forces that are orthogonal to the direction of motion.

Nelson [5] used a bulk-flow model to develop the first complete analysis for determining rotordynamic-coefficients of smooth-bore annular gas seals. His model included the continuity equation, axial and circumferential momentum equations, the energy equation, and the ideal gas law as the equation of state. He used Hirs' turbulent lubrication model [6] to define shear forces at the stator and rotor walls in terms of a Blasius [7] friction-factor model. Elrod et al. [8,9] modified Nelson's model by changing the entrance-loss factor model. Ha and Childs [10] used extensive measurements of friction factors for honeycomb surfaces to develop a new empirical friction factor model for Nelson's model. However, when compared to measured results from Pelletti and Childs [11], this modified model made only modest improvements in the direct stiffness prediction.

In the authors' response to comments on the paper by Ha and Childs [10], Childs introduced a new two-control-volume to account for the gas volume that is ''trapped'' in the honeycomb cells. No axial or circumferential flow is possible in this second control volume; only transient radial flow is permitted between the two control volumes. This model included a continuity equation, momentum equations, and the energy equation for both control volumes. Physically, the additional control volume acts to sharply reduce the effective acoustic velocity for wave propagation through the seal, and drops the acoustic natural frequencies dramatically.

Kleynhans and Childs [12] developed a perturbation solution

Contributed by the Tribology Division for publication in the ASME JOURNAL OF TRIBOLOGY. Manuscript received by the Tribology Division February 20, 2001; revised manuscript received August 15, 2001. Associate Editor: S. Wu.

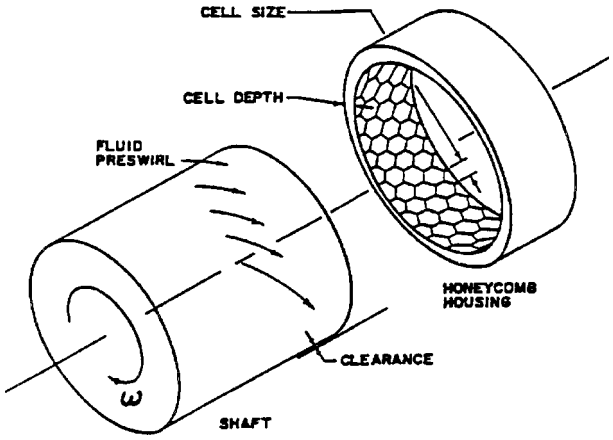

Fig. 1 Honeycomb-Stator/Smooth-Rotor seal configuration, Childs [1]

for the two-control-volume model (minus the energy equation). The governing equations for this reduced model are as follows.

Continuity Equation.

$$\frac{\partial}{\partial t}(\rho H)+\frac{1}{R}\frac{\partial}{\partial \Theta}(\rho UH)+\frac{\partial}{\partial Z}(\rho WH)+H_d\frac{\partial \rho}{\partial t}=0 \tag{2}$$

Axial-Momentum Equation.

$$-H\frac{\partial P}{\partial Z}=\tau_{sz}+\tau_{rz}+\rho WV+\frac{\partial}{\partial t}(\rho WH)+\frac{1}{R}\frac{\partial}{\partial \Theta}(\rho UWH)+\frac{\partial}{\partial Z}(\rho W^2H) \tag{3}$$

Circumferential-Momentum Equation.

$$-\frac{H}{R}\frac{\partial P}{\partial \Theta}=\tau_{s\Theta}+\tau_{r\Theta}+\rho UV+\frac{\partial}{\partial t}(\rho UH)+\frac{1}{R}\frac{\partial}{\partial \Theta}(\rho U^2H)+\frac{\partial}{\partial Z}(\rho UWH) \tag{4}$$

In the continuity equation, H_d is the average (over the seal-face area) cell depth. For $H_d=0$, a constant-temperature version of Nelson's model is obtained.

In contrast to Nelson's model, the two-control-volume model predicted the stiffness and damping coefficients of Eq. (1) to be strongly frequency dependent. Hence, the motion/reaction-force model of Eq. (1) was replaced with the general transfer-function model

$$-\begin{Bmatrix} F_x(i\Omega) \\ F_y(i\Omega) \end{Bmatrix}=\begin{bmatrix} \mathbf{D}(i\Omega) & \mathbf{E}(i\Omega) \\ -\mathbf{E}(i\Omega) & \mathbf{D}(i\Omega) \end{bmatrix}\begin{Bmatrix} \Delta x(i\Omega) \\ \Delta y(i\Omega) \end{Bmatrix}. \tag{5}$$

The functions **D** and **E** are defined from curve fits of the calculated radial and circumfential impedances. The frequency-dependent rotordynamic-coefficients are obtained from the general transfer function via

$$-\begin{Bmatrix} F_x(i\Omega) \\ F_y(i\Omega) \end{Bmatrix}=\begin{bmatrix} K+jC\Omega & k+jc\Omega \\ -(k+jc\Omega) & K+jC\Omega \end{bmatrix}\begin{Bmatrix} \Delta x(i\Omega) \\ \Delta y(i\Omega) \end{Bmatrix}. \tag{6}$$

Note that K, k, C, and c are now functions of the excitation frequency Ω.

A seal that is whirling at a fixed radius A with precession frequency Ω will develop dynamic radial and circumferential drag reaction force components $f_r=A(K+\Omega\cdot c)=A\cdot K_{\text{eff}}$ and $f_\theta=A(\Omega\cdot C-k)=A\cdot\Omega\cdot C_{\text{eff}}$, respectively. We can use these expressions to define effective stiffness K_{eff} and damping C_{eff} coefficients:

$$K_{\text{eff}}=K+c\Omega, \tag{7}$$

$$C_{\text{eff}}=C-\frac{k}{\Omega}. \tag{8}$$

Note, that K_{eff} and C_{eff} are also frequency dependent. As verified by past and ongoing tests at the authors' laboratory, the two-control-volume model does a much better job of predicting the rotordynamic coefficients of the honeycomb seals. Comparisons of predictions for the two-control-volume model using different friction-factor models will provide a better understanding of the model's behavior and a guide for selecting the appropriate or ''best'' models as additional rotordynamic test data becomes available.

Friction-Factor Models

Bulk-flow models have been used almost universally in annular seal analysis for turbulent incompressible and compressible flow. They do not account for variation in the shear stress for the fluid within the clearance, but account for the shear stress at the boundaries. In Hirs' [6] bulk-flow, turbulent-lubrication model, the shear stress at the stator is defined by

$$\tau_s=f_s\,\tfrac{1}{2}\rho(W^2+U^2). \tag{9}$$

Models proposed to date for defining the friction factor f_s are discussed below.

The Blasius Model [7]. Hirs used the Blasius model for pipe friction in his initial development. With this model, f_s is only a function of the Reynolds number Re and is stated,

$$f_s=n_s\,\text{Re}^{m_s}, \tag{10}$$

where for compressible flow,

$$\text{Re}=\left(\frac{P}{Z_cR_gT}\right)\frac{(2H)\sqrt{W^2+U^2}}{\mu}. \tag{11}$$

The two constants n_s and m_s define the stator friction factor and are empirically determined from experimental data. The hydraulic diameter for an annulus is $2C_r$ where C_r is the centered radial clearance. After Hirs, the hydraulic radius in Eq. (11) is $2H$, so that the Reynolds number and friction factor are functions of the local clearance H.

The Moody Model [13]. The Moody model is also based on pipe friction data, and is the following function of the local Reynolds number and relative roughness, $e/2H$ where e is the absolute roughness,

$$f=0.001375\left[1+\left(2000\frac{e}{2H}+\frac{10^6}{\text{Re}}\right)^{1/3}\right]. \tag{12}$$

For pipe flow, this model is restricted to relative roughness less then 10 percent. In general, honeycomb seals have a relative roughness in excess of 10 percent, limiting the Moody-equation effectiveness. More importantly, the Moody equation predicts a decrease in the friction factor with increasing clearance, versus flat-plate and seal test results showing the opposite outcome. Because of this discrepancy, the Moody model is not used here.

Childs and Fayolle Model [14]. For liquid seals with a hole-patterned-roughened stator, Childs and Fayolle defined a Blasius-like friction-factor model based on leakage data from a rotating annular seal at three different clearances. A least-square curve fit was used to calculate Blasius type coefficients for each clearance. The friction-factor model

$$f_s=n_s\,\text{Re}^{m_s} \tag{13}$$

was used where the coefficient n_s and exponent m_s are quadratic functions of clearance C_r. Assuming that the changes in friction factor due to a change in local clearance followed these results, n_s and m_s are stated:

$$n_s = a_0 + a_1 H + a_2 H^2, \tag{14}$$

$$m_s = b_0 + b_1 H + b_2 H^2. \tag{15}$$

The constants a_0, a_1, and a_2 are obtained from a quadratic curve-fit of n_s versus clearance C_r. Similarly, constants b_0, b_1, and b_2 are obtained from a quadratic curve-fit of m_s versus clearance C_r. In Eq. (13), the Reynolds number Re is a function of the nominal radial clearance C_r, not the local clearance H, since the data sets were obtained by varying the flowrate with the clearance held constant. Eqs. (14–15) model the dependency of f_s on H. This modeling approach will be used for honeycomb gas seals using the data collected by Ha and Childs [15]. Since suitable data are available for only two clearances, the model reduces to:

$$n_s = a_0 + a_1 H, \tag{16}$$

$$m_s = b_0 + b_1 H. \tag{17}$$

Al-Qutub, Elrod, and Coleman Model [16]. Measurements were made in a nonrotating annular-seal test rig for a honeycomb seal with a cell width of 1.59 mm and a cell depth of 1.8 mm. The results showed that the friction factor was a function of Reynolds number Re and the seal clearance C_r. The clearance effect was dominant, and the friction factor increased with increased clearance, similar to the results found by Ha and Childs [15], and Childs and Fayolle [14]. Al-Qutub et al.'s friction factor model is also based on the Blasius model and is defined by

$$f_s = \left[C1 + C2\left(\frac{H}{b}\right) \right] \mathrm{Re}^{m_s}, \tag{18}$$

where

$$C1 = 0.05126, \quad C2 = 0.5569, \quad m_s = -0.096.$$

Note: The Reynolds number Re in Eq. (18) is a function of the nominal radial clearance C_r, not the local clearance H.

Friction-Factor-Model Predictions

A Review of Friction-Factor Measurements. Ha and Childs [15] friction factor data were obtained for smooth and honeycomb surfaces. Tests were conducted for three clearances (0.25, 0.38, 0.51 mm), four cell widths (1.57, 0.79, 0.51, and 0.41 mm), and three cell depths (2.29, 3.05, 3.81 mm). In about 40 percent of the cases, the friction factor increased abruptly with increasing Reynolds numbers. (Note that this happened at Reynolds numbers on the order of 20,000 or higher.) The friction factor results used here apply for the remaining cases where the friction factor decreased slightly with increasing Reynolds number. The tests allow for independent variation of the Reynolds numbers (through changes in the pressure differential) and the clearance. Experiments show that the friction factor was sensitive to changes in the clearance, generally increasing with increasing clearance as shown in Fig. 2. The friction-factor also depended strongly on the cell width, cell depth and clearance. The ratio of honeycomb cell depth to honeycomb cell width d/b and the ratio of clearance to honeycomb cell width C_r/b were shown to be important parameters.

The present study considers a honeycomb seal with $b = 1.57$ mm and $d = 2.29$ mm. Figure 2 shows measured friction-factor data at clearances of 0.25 mm and 0.38 mm respectively with applied curve-fits corresponding to the Blasius friction-factor model of Eq. (10). The Blasius friction-factor model at 0.25 mm clearance takes the form

$$f = 0.0776\,\mathrm{Re}^{-0.1465}, \tag{19}$$

and at 0.38 clearance is

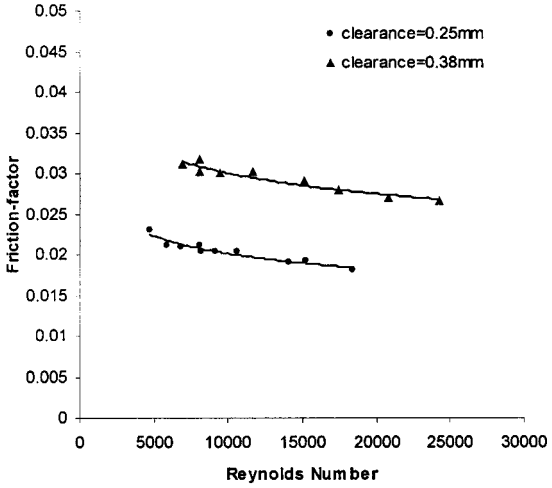

Fig. 2 Friction-factor versus Reynolds number at varying clearances, cell width 1.57 mm, and cell depth 2.29 mm; friction-factor data, Ha and Childs [15]

$$f = 0.0973\,\mathrm{Re}^{-0.1277}. \tag{20}$$

Most industrial seal applications have a clearance between 0.2 mm and 0.35 mm; hence, the 0.51 mm clearance data were not used. The Blasius model used here has the coefficients $n_s = 0.077$, $m_s = -0.1465$.

Comparisons of Friction-Factor-Model Predictions. All of the models except Ha's are variations of the Blasius model. Al-Qutub et al.'s model is similar to the Childs and Fayolle model in that n_s is a linear function of clearance; however, their exponent m_s is constant. We are interested in changes to the rotordynamic-coefficient predictions due to a change in the form of the friction-factor models, versus changes in the model's internal parameters. Since empirical constants for Al-Qutub et al.'s model are not available for honeycomb with cell depth of 2.29 mm and cell width of 1.57 mm, the data obtained by Ha and Childs [15] were used for this model's coefficients.

To obtain rotordynamic coefficients, a perturbation analysis is carried out for the governing equations, based on a small perturbation of the seal rotor about the centered position. This development requires partial derivatives of the stator friction-factor with respect to pressure, velocity, and local clearance. We will show that differences in the solutions for the Blasius, Childs and Fayolle, and Al-Qutub et al. models are mainly due to differences in the partial derivative of the stator friction-factor with respect to clearance. The partial derivatives are shown below.

Blasius Model.

$$\frac{\partial f_s}{\partial H} = m_s n_s\,\mathrm{Re}_0^{m_s}\frac{1}{C_r}, \tag{21}$$

where

$$\mathrm{Re}_0 = \left(\frac{P_0}{Z_c R_g T}\right)\frac{(2C_r)\sqrt{W_0^2 + U_0^2}}{\mu}.$$

Childs and Fayolle Model.

$$\frac{\partial f_s}{\partial H} = \mathrm{Re}_0^{(b_0 + b_1 C_r)}\left[a_1 + b_1(a_0 + a_1 C_r)\log_e \mathrm{Re}_0\right] \tag{22}$$

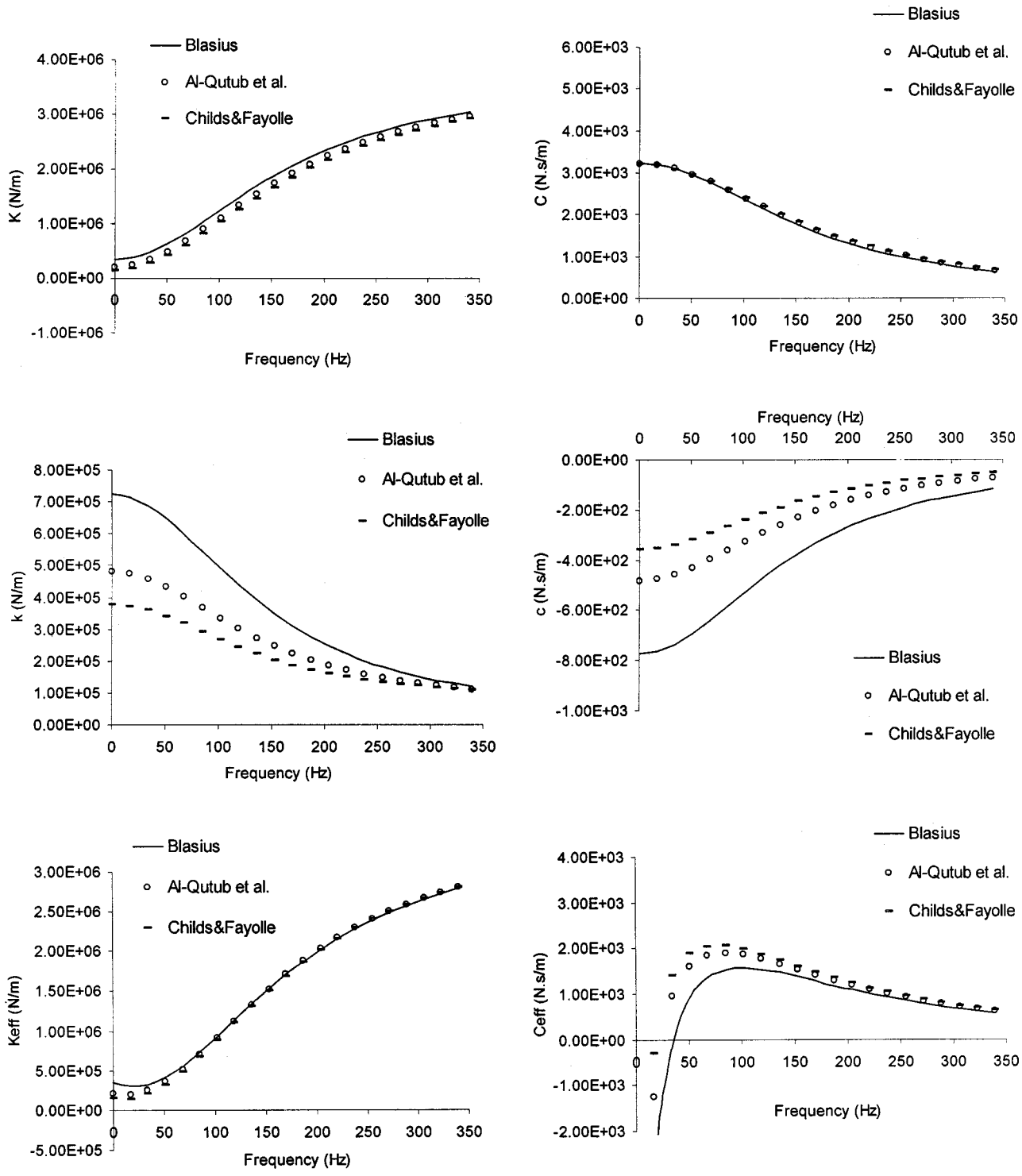

Fig. 3 Comparisons of computed rotordynamic coefficients with different friction-factor models at 10, 200 rpm, 6.89 bar inlet pressure, 0.5 pressure ratio, and clearance 0.19 mm (b=1.57 mm, d=2.29 mm)

Al-Qutub et al. Model.

$$\frac{\partial f_s}{\partial H} = \mathrm{Re}_0^{m_s}\left[\frac{C2}{b}\right] \tag{23}$$

In carrying out the partial derivatives, the Reynolds number in the Blasius model is assumed to be a function of the local clearance H. In the other two models, Re is not a function of H, but the coefficient n_s and exponent m_s are. This approach is consistent with the data taken to develop the models where the Reynolds number were varied due to changes in pressure for a range of constant clearances.

Figure 3 compares predictions for the different friction-factor models at a running speed of 10,200 rpm (170 Hz), inlet pressure 6.2 bar and 0.5 pressure ratio. The predictions nearly coincide (for all models) for the magnitudes and trends of direct stiffness K, direct damping C and effective stiffness K_{eff}. Differences arise in

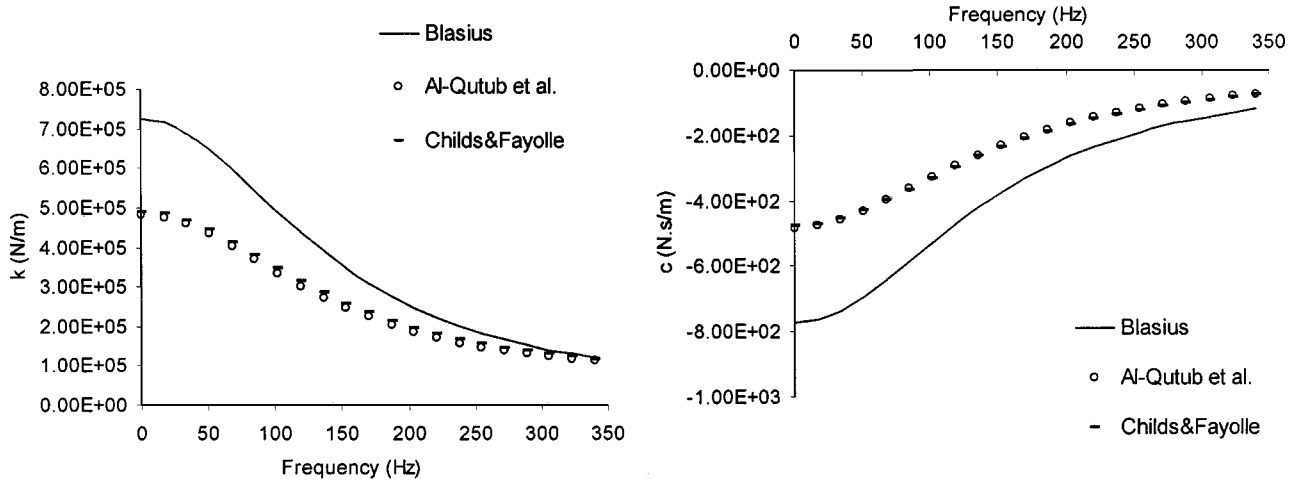

Fig. 4 Comparisons of the *k* and *c* rotodynamic coefficients using reduced (constant exponent) friction-factor models at 10, 200 rpm, 6.89 bar inlet pressure, 0.5 pressure ratio, and clearance 0.19 mm (b=1.57 mm, d=2.29 mm)

the cross-coupled stiffness k, cross-coupled damping c, and effective damping C_{eff}. Note that the magnitude of c is about 100 times smaller than the magnitude of K; hence, the different predictions for c make a minor difference in K_{eff} at low frequencies making an insignificant difference in the location of a lower critical speed. The magnitude of c is an even smaller fraction of K at higher frequencies and K_{eff} at running speeds. *Synchronous* predictions for K_{eff} can be quite important in compressor rotordynamics, since the stiffness predictions for the balance piston seal of a high-pressure injection compressor are comparable to the bearing stiffnesses.

Differences in predictions for C_{eff} arise from the differing predictions for k. The Blasius model predicts a higher k value than the other models, resulting in a lower prediction for C_{eff} at low frequencies (60~70 Hz). The predictions for C_{eff} at running speed (170 Hz) basically coincide; hence to the extent that synchronous response depends on C_{eff}, all predictions would coincide. The difference in predictions for C_{eff} arising at lower frequencies is important in regards to stability predictions, since unstable motion is generally associated with a rotor's first natural frequency. Obviously, higher predictions for C_{eff} at low frequencies would yield predictions of a more stable mode. In trying to stabilize compressors, the honeycomb cell depth is generally varied in an attempt to maximize damping at the (subsynchronous) first natural frequency.

Differences in predictions for the Blasius-type models of Childs and Fayolle, and Al-Qutub et al. arise because of the coefficients n_s and m_s depend on local clearance with partial derivatives as presented in Eqs. (22) and (23). Absent this dependency, both model reduce to the original Blasius model. Predictions for k and c using a reduced Childs and Fayolle model (constant m_s values only) and the Al-Qutub model are shown in Fig. 4 and basically coincide. Predictions for the reduced models (constant n_s and m_s values) of Childs and Fayolle, and Al-Qutub et al. models are shown in Fig. 5. As expected, the predictions for k and c from the reduced models are very close to the Blasius model at all frequencies.

Summary and Conclusions

Except for c and k, all friction-factor models predict the same rotordynamic coefficients. Different predictions for c will have minimal influence on the predicted rotordynamic response. Different predictions for k resulted in appreciable differences for C_{eff} predictions in the 60~70 Hz range. Accurate C_{eff} predictions are

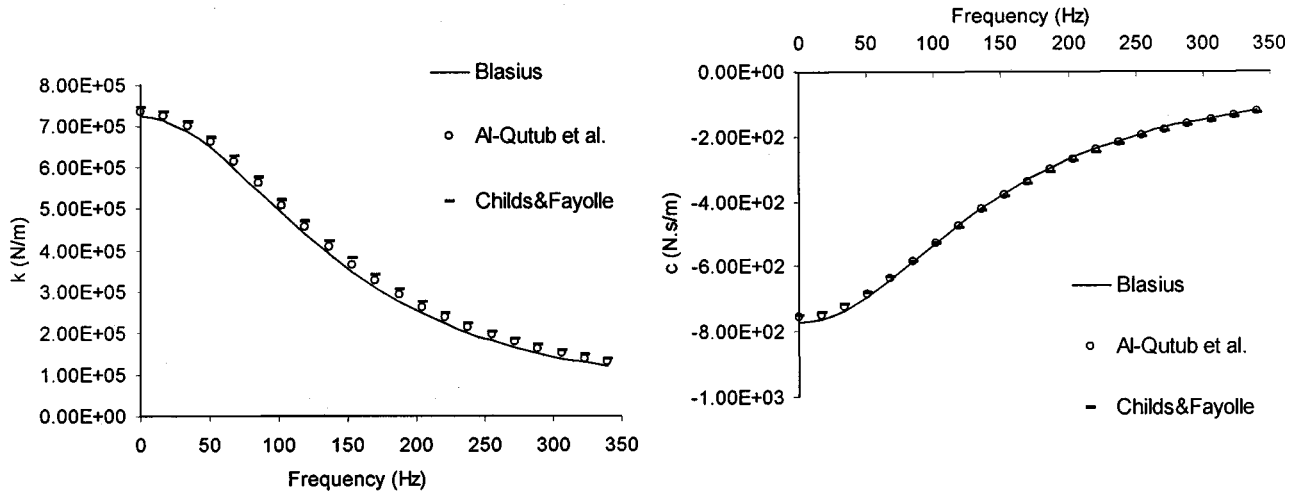

Fig. 5 Comparisons of the *k* and *c* rotodynamic coefficients using reduced (constant coefficient and exponent) friction-factor models at 10, 200 rpm, 6.89 bar inlet pressure, 0.5 pressure ratio, and clearance 0.19 mm (b=1.57 mm, d=2.29 mm)

particularly important in this frequency range because of stability considerations in centrifugal compressors, and the Childs-Fayolle model predicts higher values than the Al-Qutub et al. models. At higher frequencies, predictions for K_{eff} and C_{eff} tend to converge for all of the models.

Nomenclature

b = honeycomb cell width [L]
C, c = direct and cross-coupled damping coefficients [FT/L]
C_{eff} = effective damping coefficient [FT/L]
C_r = seal radial clearance [L]
d = honeycomb cell depth [L]
$\mathbf{D}$ = direct impedance [F/L]
e = absolute surface roughness height [L]
$\mathbf{E}$ = cross-coupled impedance [F/L]
f_s = friction factor of stator
Fx, Fy = components of seal reaction force [F]
H = local clearance [L]
H_d = effective honeycomb cell depth [L]
K, k = direct and cross-coupled stiffness coefficients [F/L]
K_{eff} = effective stiffness coefficient [F/L]
Ma = Mach number
n = Blasius friction factor coefficient
m = Blasius friction factor exponent
P = pressure [F/L^2]
P_c = critical pressure of air [F/L^2]
R = seal radius [L]
R_g = gas constant [LF/MT]
Re = Reynolds number
U = circumferential bulk fluid velocity [L/T]
W = axial bulk fluid velocity [L/T]
x, y = relative displacement between stator and rotor [L]
$\dot{x}, \dot{y}$ = relative velocity between stator and rotor [L/T]
Z = axial coordinate [L]
Z_c = gas compressibility factor
μ = fluid viscosity [FT/L^2]
τ = shear stress [F/L^2]
ω = rotor rotational frequency [1/T]
Ω = rotor precession frequency [1/T]
Θ = circumferential coordinate

Subscripts

r, s = denotes rotor and stator
0 = parameters calculated at $H = C_r$

References

[1] Childs, D., 1993, *Turbomachinery Rotordynamics: Phenomena, Modeling, and Analysis*, John Wiley & Sons, Inc., New York, NY, pp. 293.
[2] Childs, D., and Moyer, D., 1985, "Vibration Characteristics of the HPOTP (High-Pressure Oxygen Turbopump) of the SSME (Space Shuttle Main Engine)," ASME J. Eng. Gas Turbines Power, **107**, No. 1, pp. 152–159.
[3] Zedian, F., Perez, R., and Stephenson, M., 1993, "The Use of Honeycomb Seals in Stabilizing Two Centrifugal Compressors," *Proceedings of the Twenty-Second Turbomachinery Symposium*, Turbomachinery Laboratory, Texas A&M University, College Station, TX, pp. 3–15.
[4] Armstrong, J., and Perricone, F., 1996, "Turbine Instability Solution-Honeycomb Seals," *Proceedings of the Twenty-Fifth Turbomachinery Symposium*, Turbomachinery Laboratory, Texas A&M University, College Station, TX, pp. 47–56.
[5] Nelson, C., 1985, "Rotordynamic Coefficients for Compressible Flow in Tapered Annular Seals," ASME J. Tribol., **107**, pp. 318–325.
[6] Hirs, G., 1973, "A Bulk-Flow Theory for Turbulence in Lubricating Films," ASME J. Lubr. Technol., pp. 137–146.
[7] Blasius, H., 1913, "Das Ahnlichkeitsgesetz bei Reibungsvorgängen in Flüssigkeiten," Forschg. Arb Ing.-Wes., Heft 131, Berlin.
[8] Elrod, D., Nelson, C., and Childs, D., 1989, "An Entrance Region Friction Factor Model Applied to Annular Seals Analysis: Theory Versus Experiment for Smooth and Honeycomb Seals," ASME J. Tribol., **111**, pp. 337–343.
[9] Elrod, D., Childs, D., and Nelson, C., 1990, "An Annular Gas Seal Analysis Using Empirical Entrance and Exit Region Friction Factors," ASME J. Tribol., **112**, No. 2, pp. 196–204.
[10] Ha, T., and Childs, D., 1994, "Annular Honeycomb-Stator Turbulent Gas Seal Analysis Using New Friction-Factor Model Based on Flat Plate Tests," ASME J. Tribol., **116**, pp. 352–360.
[11] Pelletti, J., and Childs, D., 1991, "A Comparison of Experimental Results and Theoretical Predictions for the Rotordynamic Coefficients of Short ($L/D = 1/6$) Labyrinth Seals," Proceedings, *1991 ASME Design Technical Conference*, September, DE-Vol-35, pp. 69–76.
[12] Kleynhans, G., and Childs, D., 1997, "The Acoustic Influence of Cell Depth on the Rotordynamic Characteristics of Smooth-Rotor/Honeycomb-Stator Annular Gas Seals," ASME J. Eng. Gas Turbines Power, **119**, pp. 949–957.
[13] Moody, L. F., 1944, "Friction Factors for Pipe Flow," Trans. ASME, **66**, pp. 671–684.
[14] Childs, D., and Fayolle, P., 1999, "Test Results for Liquid 'Damper' Seals Using a Round-Hole Roughness Pattern for the Stators," ASME J. Tribol., **121**, No. 1, pp. 42–49.
[15] Ha, T. H., and Childs, D., 1991, "Friction Factor Data for Flat-Plate Tests of Smooth and Honeycomb Surfaces (Including Extended Test data)," Texas A&M University, Turbomachinery Laboratory Reports, TL-SEAL-1-91.
[16] Al-Qutub, A., Elrod, D., and Coleman, H., 1999, "A New Friction Factor Model and Entrance Loss Coefficient For Honeycomb Annular Gas Seals," ASME J. Tribol., **22**, No. 3, pp. 622–627.